Allosteric Inhibition of the Protein-Protein Interaction between the Leukemia-Associated Proteins Runx1 and CBFβ

Michael J. Gorczynski,[1,7] Jolanta Grembecka,[2] Yunpeng Zhou,[2] Yali Kong,[3] Liya Roudaia,[4] Michael G. Douvas,[5] Miki Newman,[2] Izabela Bielnicka,[2] Gwen Baber,[2] Takeshi Corpora,[2] Jianxia Shi,[2,8] Mohini Sridharan,[6] Ryan Lilien,[6] Bruce R. Donald,[6,9] Nancy A. Speck,[4] Milton L. Brown,[3,*] and John H. Bushweller[2,*]

[1]Department of Chemistry, University of Virginia, Charlottesville, VA 22904, USA
[2]Department of Molecular Physiology and Biological Physics, University of Virginia Health Sciences, Charlottesville, VA 22908, USA
[3]Department of Oncology, Drug Discovery Program, Georgetown University Medical Center, Washington, DC 20057, USA
[4]Department of Biochemistry, Dartmouth Medical School, Hanover, NH 03755, USA
[5]Department of Medicine, University of Virginia Health System, Charlottesville, VA 22908, USA
[6]Department of Computer Science, Dartmouth College, Hanover, NH 03755, USA
[7]Present address: Department of Chemistry, Wake Forest University, Winston-Salem, NC 27109, USA.
[8]Present address: Amgen, Incorporated, Thousand Oaks, CA 91320, USA.
[9]Present address: Department of Computer Science, Duke University Medical Center, Durham, NC 27708, USA.
*Correspondence: mb544@georgetown.edu (M.L.B.), jhb4v@virginia.edu (J.H.B.)
DOI 10.1016/j.chembiol.2007.09.006

SUMMARY

The two subunits of core binding factor (Runx1 and CBFβ) play critical roles in hematopoiesis and are frequent targets of chromosomal translocations found in leukemia. The binding of the CBFβ-smooth muscle myosin heavy chain (SMMHC) fusion protein to Runx1 is essential for leukemogenesis, making this a viable target for treatment. We have developed inhibitors with low micromolar affinity which effectively block binding of Runx1 to CBFβ. NMR-based docking shows that these compounds bind to CBFβ at a site displaced from the binding interface for Runx1, that is, these compounds function as allosteric inhibitors of this protein-protein interaction, a potentially generalizable approach. Treatment of the human leukemia cell line ME-1 with these compounds shows decreased proliferation, indicating these are good candidates for further development.

INTRODUCTION

The protein-protein interaction between the subunits of the heterodimeric transcription factor CBF, core binding factor β (CBFβ), and Runx1 (CBFα) plays a critical role in hematopoiesis (blood cell development) [1]. CBFβ functions to increase the DNA binding of the Runx1 subunit 20- to 40-fold [2] and to protect the Runx1 subunit against ubiquitination and subsequent proteasome degradation [3]. The gene coding for the CBFβ subunit (CBFB) is the target of a common chromosomal translocation, inv(16), found in 12%–15% of acute myeloid leukemia cases [4]. This translocation results in the fusion of the N-terminal 165 amino acids of CBFβ to the coiled-coil region of smooth muscle myosin protein (hereafter referred to as CBFβ-SMMHC). The CBFβ-SMMHC fusion protein causes dysregulation of CBF function [5] in part by means of anomalously tight binding to Runx1 [6]. Because binding to Runx1 is required for the dysfunction associated with this protein, this binding represents an excellent target for inhibition as a potential therapeutic strategy. A small-molecule inhibitor of this kind has the potential to be a useful and highly specific therapeutic agent. We have developed small molecules which bind to CBFβ and inhibit Runx1 binding. This represents the first step toward our overall goal of developing compounds which can specifically inhibit CBFβ-SMMHC while minimally perturbing the activity of CBFβ itself.

Although there is a long history of development of small-molecule inhibitors of enzymes by means of targeting their active sites, the development of inhibitors of protein-protein interactions has been relatively limited [7–10]. Potential difficulties in developing inhibitors of protein-protein interactions include the large surface area typically buried at such interfaces, the lack of significant curvature on these interfaces [7], and the increased mobility of the side chains and often the backbone at these interfaces [11, 12]. Recent successes in the development of small-molecule inhibitors of protein-protein interactions [7–10, 13–17] suggest these barriers are surmountable. Mutagenesis studies of protein interfaces have clearly demonstrated that only a small subset of amino acids at a particular interface contributes the vast majority of the binding energy. These results clearly imply that targeting of molecules to these so-called hot spots is highly likely to disrupt the interaction and that extensive coverage of the protein interface with relatively large molecules is not required. Indeed, recent success in the development of protein-protein inhibitors targeting Rac1 [13] and Bcl-2 [14] bodes well for structure-based approaches to this. An intriguing

alternative approach is the development of allosteric inhibitors [18] of protein-protein interactions in which the molecule would bind at a site offset from the protein-protein interface and thereby not have to compete with the binding partner. Indeed, examples of such allosteric inhibitors have been demonstrated for β-lactamase [19], LFA-1 [20], and nitric oxide synthase [21], suggesting this may be a generalizable approach.

We have solved the 3D structure of CBFβ using solution NMR [22] and mapped the binding interface with Runx1 by both chemical shift perturbation as well as Ala mutagenesis of the binding interface [23]. This provided the framework to carry out virtual screening, and subsequent screening by chemical shift perturbation in 2D ^{15}N-^{1}H HSQC spectra of CBFβ to identify potential lead compounds. A FRET-based assay and an ELISA have been developed to measure the effectiveness of these compounds in inhibiting the CBFβ-Runx1 Runt domain interaction. Using a traditional medicinal chemistry approach, we have elaborated these compounds to identify structure-activity relationships, resulting in compounds with significant inhibitory potency (low micromolar range). We have used the NMR chemical shift perturbations to dock the compounds to CBFβ and show that they bind at a site offset from the interfacial region of CBFβ. These data show that they act in an allosteric manner to inhibit the binding of Runx1 to CBFβ. These inhibitors demonstrate activity in a cellular FRET assay in HEK293 cells and inhibition of proliferation of the leukemia cell line ME-1 (containing the inv[16]), indicating they are good leads for further development.

RESULTS

Lead Identification and NMR Chemical Shift Perturbation Screening

The computer program LUDI/InsightII (Accelrys) [24, 25] has been utilized for virtual screening using the Available Chemicals Directory database of ~70,000 commercially available compounds with drug-like properties. The 20 conformers of CBFβ used to represent the solution structure of the protein were employed for virtual screening, which resulted in 35 compounds selected for experimental screening using NMR spectroscopy. Screening by means of observation of chemical shift changes in the 2D ^{15}N-^{1}H or ^{13}C-^{1}H HSQC spectra of proteins in the presence of ligands has been very successfully applied [26–29]. In this study, we have employed chemical shift perturbations in the 2D ^{15}N-^{1}H HSQC spectra of CBFβ in the presence of ligands to identify compounds that bind to the protein as well as to provide information on the location of their binding site. Four of the 35 compounds showed significant chemical shift changes in 2D ^{15}N-^{1}H HSQC spectra of CBFβ. Data for one of the four are shown in Figure 1A. The structures of these four molecules (Table 1, compounds **1–4**) share a common substructure, namely a 2-aminothiazole attached to an aromatic ring. We also titrated CBFβ with each of the initial compounds to get an estimate of the binding constant, which showed they
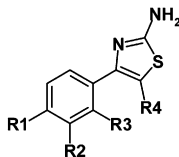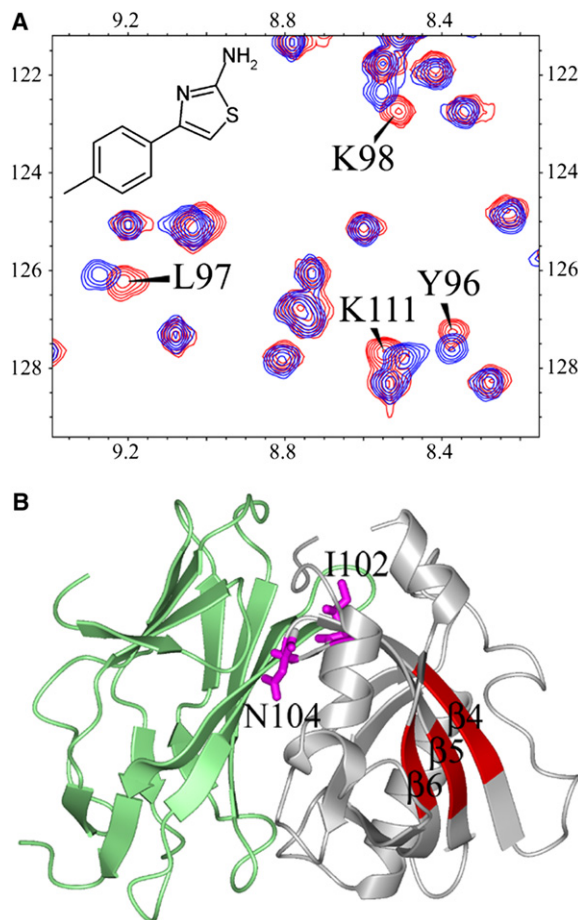

Figure 1. Interactions of 2 with CBFβ
(A) Selected region of the ^{15}N-^{1}H HSQC spectrum of CBFβ (red) and CBFβ plus **2** (blue). Amides perturbed upon binding are labeled.
(B) Residues with chemical shift perturbations (red) mapped onto the structure of CBFβ (gray) complexed to the Runx1 Runt domain (green). The side chains of N104 and I102 are shown in magenta.

all bind with low millimolar dissociation constants. Because we have previously assigned the NMR spectra of CBFβ, these data also provide an indication of the binding site on CBFβ. Figure 1 shows the chemical shift perturbations observed for one of the lead compounds mapped onto the structure of CBFβ. Interestingly, the observed perturbations are consistent with binding at a site displaced from the Runx1 interface (Figure 1B). Because these lead compounds are not binding directly at the interface, any inhibitory effects of these compounds would necessarily have to occur by means of an allosteric or noncompetitive mechanism.

FRET Assay

In order to assess the effectiveness of these compounds in inhibiting binding of the Runx1 Runt domain to CBFβ, we have developed a FRET assay to measure this binding (Figures 2A and 2B). We fused the green fluorescent protein derivative Cerulean to the N terminus of the Runt

Table 1. Results of FRET and ELISA Experiments

Compound	R1	R2	R3	R4	IC$_{50}$ (μM)	IC$_{50}$ ELISA (μM)
1	H	H	H	H	ND 27[a]	ND
2	Me	H	H	H	ND 10[a]	ND
3	Me	H	Me	H	ND 12[a]	ND
4	H	H	CH-CH		ND 9[a]	ND
5	CF$_3$	H	H	H	9.0 ± 1.4	3.0 ± 0.1
6	OMe	H	H	H	18.5 ± 3.5	12 ± 1.4
7	OMe	OMe	H	H	40.5 ± 4.9	18 ± 2.8
8	O-CH$_2$-O		H	H	9.0 ± 1.4	6.5 ± 0.7
9	H	Cl	H	H	12.0 ± 1.4	6.5 ± 2.1
10	H	Me	H	H	110 ± 12	36 ± 10
11	H	OMe	H	H	61 ± 3.0	22.5 ± 2.1
12	H	OCF$_3$	H	H	ND 19[a]	>700
13	H	H	Me	H	5 ± 0.0	3.3 ± 0.5
14	H	H	Cl	H	1.1 ± 0.14	0.7 ± 0.2
15	H	H	OMe	H	ND 5[a]	>1000
16	Cl	H	Cl	H	49 ± 15	20.5 ± 0.7
17	OMe	H	H	Et	3.2 ± 0.3	3.5 ± 0.7
18	OMe	H	H	Propyl	23.5 ± 1.5	3.2 ± 0.3
19	H	Me	H	Et	66 ± 2.0	16.5 ± 4.9
20	H	H	OMe	Et	17 ± 2.8	18 ± 4.2
21	OEt	H	H	Et	>500	>500

ND, not determined due to weak binding.
[a] Percent inhibition observed at 250 μM ligand concentration.

domain and the green fluorescent protein derivative Venus to the N terminus of CBFβ. The ratio of the emission intensities at 525 nm and 474 nm was used as the readout in this assay. We have validated the assay by determining the K$_d$ for binding using serial dilution resulting in a K$_d$ value of 87 nM (data not shown), in very good agreement
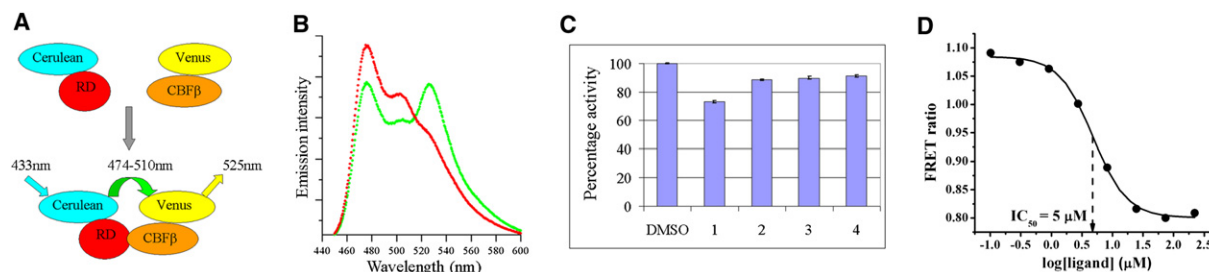
Figure 2. FRET Assay
(A) Schematic of FRET experiment.
(B) Fluorescence emission spectra (433 nm excitation) for a Cerulean-Runt domain/Venus-CBFβ complex (green) and for the Cerulean-Runt domain/Venus-CBFβ complex plus a 10-fold excess of CBFβ (red).
(C) Results of FRET assay for 1–4 at 250 μM ligand concentration. Error bars represent the mean ± standard deviation of two replicates.
(D) Activity (IC$_{50}$) calculated from the FRET ratio (Emission$_{525}$/Emission$_{474}$) as a function of ligand concentration (μM) for 13.
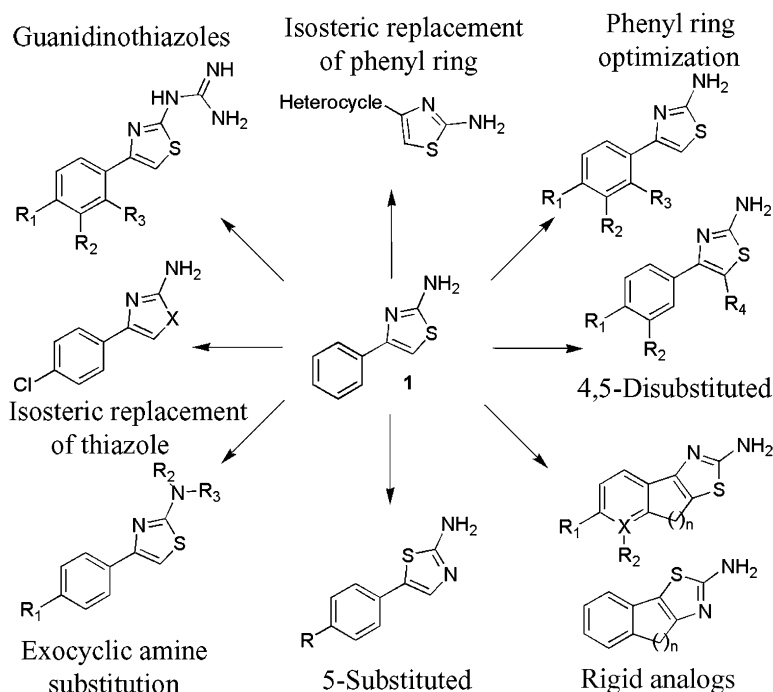
Figure 3. Design of Library for SAR Analysis

with the K_d value of 57 nM obtained from calorimetric measurements of the binding of unmodified Runt domain to unmodified CBFβ [6]. The four lead compounds identified from the NMR screen were tested using this FRET assay at a compound concentration of 250 μM (Figure 2C). One of the four (1) showed ∼30% inhibition and the remaining three (2–4) exhibited weak inhibition (∼15%) of the interaction between the two proteins, thus validating these compounds as potential leads for further development. The dynamic range for the FRET assay was determined by adding a 20-fold excess of untagged CBFβ to the assay, and the associated change in the FRET ratio was defined as 100% inhibition.

Design and Synthesis of a Compound Library for SAR
Based on the core scaffold of compound 1, we systematically designed a targeted set of compounds to explore the structure-activity relationships (SAR) for these inhibitors. Initial efforts focused on the generation of a library of 2-aminothiazoles to explore electronics, sterics, conformation, and hydrogen bonding and resulted in the synthesis and screening of over 100 compounds, resulting in 17 active compounds (Table 1). Structural information for a select number of these compounds is illustrated in Figure 3. In general, thiazoles 4–21 were synthesized using a modified Hantzsch thiazole reaction [30, 31] in 27%–99% yield. Details of the syntheses are provided in Supplemental Data available with this article online.

Results of NMR, FRET, and ELISA Assays
The synthesized compounds were screened by NMR and by FRET. NMR screening was used to identify compounds that bound to CBFβ as well as the site of binding. FRET assays were then employed to assess inhibitory effectiveness. The most frequently and most substantially perturbed residues in the NMR spectra are Y96, L97, K98, A99 (β4), and G112 (β5) as well as G123 and C124 (β6), confirming the binding of these molecules at a site displaced from the heterodimerization interface (Figure 1B). In addition, for many of the compounds, we observed chemical shift perturbations at the heterodimerization interface in the vicinity and/or at the energetic hot spots for CBFβ binding to the Runx1 Runt domain (N63, L64, Q67, L103, N104). This suggests that despite the fact that these compounds bind at a site displaced from the protein-protein interface, they do affect the conformation and/or dynamics of residues at the interface, resulting in inhibition of the CBFβ-Runx1 interaction (see Discussion for details).

In order to obtain the more quantitative characterization necessary to guide efforts to optimize these compounds, we have measured the IC_{50} for all compounds by FRET and ELISA assays. A representative plot from a FRET assay is shown in Figure 2D and inhibition data for 21 active compounds is tabulated in Table 1. Several of these compounds are very effective in inhibiting the CBFβ-Runx1 interaction, five of which have IC_{50} values below 10 μM, including 14 and 17 with IC_{50} values of 1.1 μM and 3.2 μM, respectively. All active compounds were also tested in the presence of detergent (0.1% Triton X-100) to exclude the possibility of promiscuous inhibition by aggregate (micelle) formation [32].

In order to confirm the activity of these compounds by an independent method, we have developed an ELISA assay to evaluate their effectiveness as well. IC_{50}s determined by ELISA correlate very well (R = 0.91) with the FRET data (Table 1) with no more than 3-fold differences
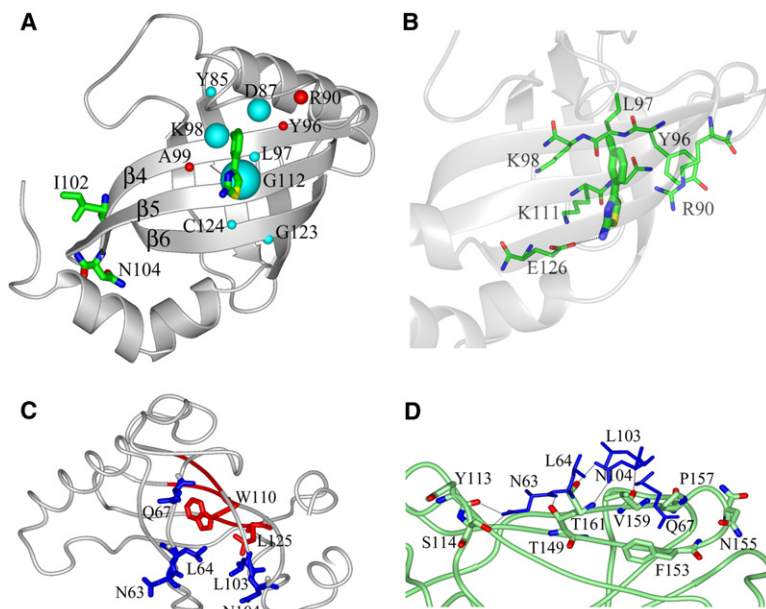
Figure 4. Binding Mode of 10 Interacting with CBFβ Calculated Using SDILICON

(A) The observed NMR chemical shift perturbations (CSP) for the amide protons of the protein: cyan balls indicate positive CSP (downfield shift) and red balls represent negative changes (upfield shift) upon ligand binding. The ball radius is proportional to the magnitude of the CSP. Side chains of I102 and N104 are shown in stick representation. The C-terminal α helix (residues 128–135) was removed for clarity.

(B) Side chains of CBFβ residues interacting with 10 are shown in stick representation (C, green; O, red; N, blue; S, yellow).

(C) CBFβ residues with CSP at the heterodimerization interface (blue). Ligand binding site and side chains of two residues from this region (W110 and L125) involved in intramolecular interactions with perturbed residues from the heterodimerization interface are in red.

(D) Side chains of CBFβ residues with CSP (blue) and their interactions with the Runt domain (green) (amino acids involved in interactions with CBFβ are colored according to atom types: C, green; O, red; N, blue).

in IC$_{50}$ values obtained by both methods, confirming the reliability of the methods we applied for inhibition measurement. The only exceptions are compounds **18** and **19**, which had IC$_{50}$ values 7.5-fold and 4-fold lower, respectively, when measured by ELISA versus FRET.

NMR-Based Docking of Ligands

CBFβ has not been successfully crystallized as of yet as a single protein, so we obtained data from NMR chemical shift perturbation studies to determine the binding mode for the inhibitors on CBFβ. We have used the approach previously described by McCoy and Wyss [33, 34] and implemented in the SDILICON program (http://tonga.usip.edu/gmoyna/sdilicon/sdilicon.c/). NMR chemical shift perturbations (CSP) for two compounds (**10** and **8**), selected based on their favorable solubility properties at high concentrations, were used to guide the docking to CBFβ. The LigandFit/Cerius2 program was used first to find initial ligand "poses" in the protein binding site, followed by SDILICON calculations to further optimize ligand orientation and conformation. Out of seven poses for **10**, two of them (indicated as clusters 2 and 4 in Table S1) clearly showed the best agreement between calculated and experimental CSP values. The values calculated by SDILICON (final shift deviation and shift penalty energy contribution) were better for binding mode 2, suggesting this binding mode as the most probable orientation of **10** in the binding site. Nevertheless, both orientations were selected for further analysis to identify the correct ligand binding mode. These binding modes differ only in their reversed orientation in the binding site (Figure S1). The same result was obtained for **8**, where five starting ligand orientations were used as input for the CSP calculations, and two with the lowest energy showed the best agreement between calculated and measured CSP values. In both

binding modes, **8** occupies the same area of the binding site as **10**, and these binding modes superimpose very well with the two most probable orientations of **10** in the CBFβ binding site. The same binding modes obtained as a result of calculations for two different CBFβ ligands strongly suggests that the core pharmacophore, that is, the phenyl and thiazole rings, occupies the same site for all the ligands derived from this core. This assumption is strongly supported by the observation of NMR chemical shift perturbations for amino acids in this binding site for all of the ligands with this core scaffold. In order to distinguish between the two proposed binding modes, the potential interactions of all ligands with CBFβ were analyzed based on the positions of the "core" fragments taken from binding mode 2 and binding mode 4 of **10**. Ligands were examined for potential steric conflicts as well as affinity differences to distinguish between the two modes. This analysis is clearly only consistent with binding mode 2 (Figures 4A and 4B). This is in good agreement with the CSP calculations, which showed much lower differences between the calculated and measured values for this binding mode (correlation coefficient: R = 0.95; see Figure S2). In addition, positive CSP values are observed for all amide protons which are in the plane of these aromatic rings, whereas negative values are observed for the amide protons above the plane (Figure 4A), again consistent with this binding mode. All these findings make ligand binding mode 2 (Figures 4A and 4B) very reliable and make possible further analysis of ligand-protein interactions based on this binding mode.

The binding site on CBFβ for these compounds employs the residues of the loop connecting β3 with β4 and three β strands: β4, β5, and β6 (Figures 4A and 4B), and is localized on the protein surface. This protein cleft is not involved in the binding of CBFβ to the Runt domain, as
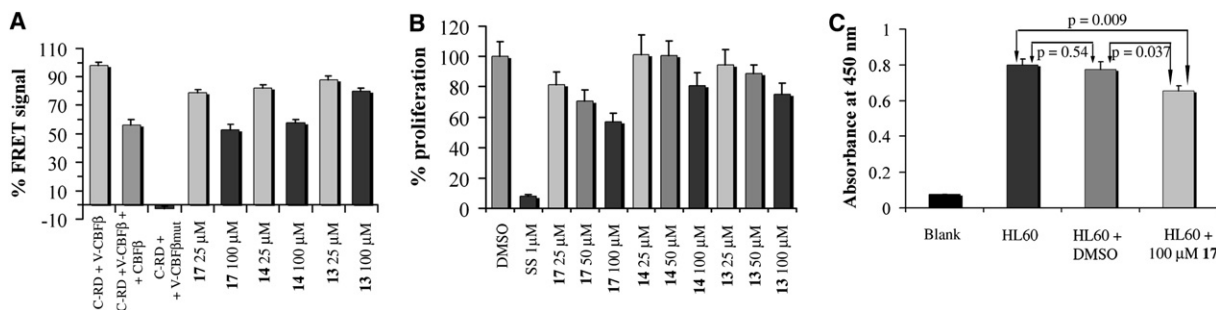
Figure 5. Biological Effects of Compounds

(A) Activity of compounds in the in vivo FACS/FRET assay. Compounds were added to Venus-CBFβ (V-CBFβ)- and Cerulean-Runt domain (C-RD)-expressing cells at 25 μM and 100 μM concentrations, while all controls were treated with 1% DMSO for 5 hr. C-RD + V-CBFβ represents HEK293 cells expressing Venus-CBFβ and Cerulean-Runt and was defined as a 100% FRET signal. C-RD + V-CBFβ + CBFβ refers to cells expressing Venus-CBFβ, Cerulean-Runt, and CBFβ and was defined as 50% FRET. C-RD + V-CBFβmut refers to cells expressing Venus-CBFβ G61A/N104A and Cerulean-Runt and was defined as 0% FRET. Bars represent mean percent FRET values ± 95% confidence intervals based on a regression line derived from positive and negative control values. All treatments and negative controls were statistically significant (p < 0.001) in comparison with the C-RD + V-CBFβ control in an unpaired, two-tailed t test. The graph represents combined data from three independent experiments, with triplicate to quintuplicate samples per treatment in each experiment.

(B) Effect of compounds on proliferation of ME-1 cells measured after 72 hr using an MTT assay. Absorbance measured at 570 nm for cells treated with 0.25% DMSO was defined as 100% proliferation (0.25% DMSO had no effect on growth) and all data were normalized with respect to this. The graph represents mean values and standard deviations for combined data from two independent experiments, each performed in quadruplicate. Staurosporine (SS) was used as a positive control for inhibition of proliferation.

(C) Results of an ELISA for Runx1 DNA binding in HL60 nuclear extracts after treatment with **17**. Each experiment was repeated five times and data shown are the mean ± SD.

mentioned above. The bottom of the binding site is formed by the backbone atoms of the residues originating from these strands, with the amino acids of β4 (Y96, L97, K98) and β5 (K111, G112) being in closest proximity to the ligand (Figures 4A and 4B). The majority of the interactions between the protein and the ligand involve the side chains of various CBFβ residues. The side chains of K98 and K111 on one side and Y96 and R90 from the other side define the shape and spatial arrangement of the binding cavity, which remains open to the solvent (Figure 4B). The thiazole ring interacts with the hydrophobic portion of the K111 side chain. A hydrogen bond is expected between the carboxyl group of E126 and the amino group attached to the thiazole ring. The phenyl ring of the ligand is inserted between the side chains of K98 and Y96, both being involved in hydrophobic interactions with this ring. In addition, the guanidine group of Arg90 is in proximity to both aromatic rings of **10**, particularly the phenyl ring (distance <4 Å), making it possible for π-cation interactions between these groups. The methyl group at the meta position of the phenyl ring in **10** is directed at the backbone of L97 (Figure 4B) and is surrounded by the backbone atoms of the residues 96–98. The meta-methyl group is involved in hydrophobic interactions with the K98 and Y96 side chains.

FACS/FRET Analysis of Inhibition in HEK293 Cells
In order to test the cell permeability of these compounds as well as their ability to disrupt the CBFβ-Runx1 interaction in mammalian cells, we utilized a fluorescence-activated cell sorting-fluorescence resonance energy transfer (FACS/FRET) method [35–37]. FACS/FRET provides the advantages of high-throughput screening of cells

with specific levels of expression of fluorescent proteins while avoiding drawbacks common to FRET microscopy methods such as photobleaching and the effects of transfection efficiency. Although FACS/FRET has been successfully used previously to assess extra- and intracellular protein-protein interactions [36, 38–41], this is, to our knowledge, its first application for screening compounds which disrupt protein-protein interactions. We performed the screen on suspension human embryonic kidney 293 (HEK293) cells which were transiently transfected with plasmids expressing Cerulean-Runt and Venus-CBFβ, or the negative control Venus-CBFβ G61A/N104A mutant, which has more than 100-fold lower affinity for the Runt domain [6, 23]. Alternatively, cells were transfected with Cerulean-Runt-, Venus-CBFβ-, and CBFβ-coding plasmids, the last as an approximately 50% competition control. Two days posttransfection, cells were incubated with compounds at 25 or 100 μM concentrations or 1% DMSO vehicle as control for 5 hr to allow for energy-dependent or -independent uptake. We measured FRET output from cells expressing equivalent uniform levels of Venus-CBFβ, as Cerulean emission may fluctuate upon disruption of Runt and CBFβ interaction. The three tested compounds decreased FRET emission in a concentration-dependent manner with high statistical significance (see Figure 5A). At the 100 μM concentration, the FRET signal was 52.7% ± 7.1, 57.8% ± 4.9, and 79.7% ± 4.5 of control for compounds **17**, **14**, and **13**, respectively. Compound **17** displayed the highest activity, and its inhibition of the Runt domain-CBFβ interaction was quite comparable to the decrease observed in the CBFβ competition control. Importantly, we saw no evidence of toxicity to the cells upon compound treatment.

Effect of 17 on ME-1 Cells and Other Mammalian Cell Lines

In order to probe the potential efficacy of the compounds for inv(16) leukemia, we have tested their ability to inhibit proliferation of ME-1 cells, a leukemia cell line expressing CBFβ-SMMHC, product of the inv(16). ME-1 [42, 43] cells were treated with a single dose of compound at various concentrations (0, 25, 50, 100 μM) and assayed for inhibition of proliferation by MTT (3-[4,5-dimethylthiazol-2-yl]-2,5-diphenyltetrazolium bromide) assay 72 hr after treatment. As seen in Figure 5B, compound **17** was most active in this assay, showing a clear dose-dependent reduction in proliferation. More modest effects were seen with **13** and **14**, consistent with the FACS/FRET results in HEK293 cells, where **17** was also the most potent. As all three compounds have similar IC$_{50}$ values (Table 1), this suggests there may be differences in uptake or serum absorption among these three inhibitors.

Based on the block in proliferation of ME-1 cells seen with **17**, we sought to assess whether there is increased differentiation of ME-1 cells upon treatment with **17**. As surface markers for the differentiation of ME-1 cells are not well established, we have used changes in morphology to qualitatively assess the extent of differentiation [44]. Figure 6 shows the results of this analysis. Treatment with **17** for a 3 day period showed an increase in apoptotic cells but limited if any effects on the morphology of living cells (see Figures 6D–6F). In contrast, a 14 day treatment with **17** or **17** plus all-*trans*-retinoic acid (ATRA) (see Figures 6G–6I) resulted in cells with greater variation in size and shape, lower nuclear-to-cytoplasmic ratio, increased folding and lobation of nuclei, and more clumped chromatin. All of these morphology changes are consistent with differentiation to more mature forms.

In order to assess the general cytotoxicity of **17**, we have assayed it against several cell lines other than ME-1. Hep-G2 and HK-2 cells, derived from liver and kidney, two of the most frequent sites of toxicity in vivo, were evaluated. As seen in Figure S4, at 50 μM, **17** actually increases proliferation of Hep-G2 cells (+20%), whereas HK-2 cells are inhibited (−31%) to a similar extent as the ME-1 cells (see Figure 5). In addition, we have treated three leukemia cell lines (K562, HL60, U937) with **17** and assessed the impact on proliferation. Whereas K562 cells were not affected to any significant extent (−10%), the HL60 (−33%) and U937 (−42%) were affected to a similar extent as seen for ME-1 cells. The increased effect in HL60 and U937 cells versus K562 cells is consistent with the higher levels of Runx in HL60 and U937 and therefore potentially higher dependence on Runx function for proliferation. This inhibitor is clearly not pan-cytotoxic, making it a viable candidate for further development.

Effect of Compounds on DNA Binding by Runx1

As it is known that CBFβ enhances the DNA binding of Runx proteins [2], treatment with CBFβ inhibitors should reduce DNA binding by Runx in a cellular context. In order to test this, we have tested the effect of **17** on Runx1 DNA binding in an HL-60 nuclear extract using a Runx1 ELISA assay (Active Motif). As seen in Figure 5C, there is indeed a statistically significant reduction in Runx1 bound to DNA upon treatment with **17**.

DISCUSSION

Allosteric Inhibition of the CBFβ-Runx1 Interaction

The compounds generated by virtual screening and selected for experimental evaluation were originally expected to interact with CBFβ at the heterodimerization interface. However, we have shown by NMR spectroscopy that they bind to a novel allosteric site on CBFβ. The lack of significant curvature at the heterodimerization interface of CBFβ likely makes it difficult to design compounds which can bind there effectively. The allosteric site on CBFβ is well defined in terms of shape and amenable to binding small molecules. In fact, as a result of further virtual screening and experimental screening searches carried out to date, we have identified three additional classes of small-molecule inhibitors interacting with this allosteric site and blocking heterodimerization of CBFβ (data not shown). Despite extensive effort, we have not been able to identify a small-molecule inhibitor interacting with CBFβ at the heterodimerization interface. This is likely to be an issue that arises for other protein-protein interaction inhibitors. Our successful identification of a targetable allosteric site on CBFβ presents a potentially generalizable approach to circumvent this problem.

Structure-Activity Analysis of IC$_{50}$ Data

Using the calculated binding mode of **8** and **10** to CBFβ, we have analyzed the interactions of other inhibitors (Table 1) to gain insight into the structure-activity relations for these compounds and guide further optimization. According to this binding mode, a relatively large substituent can be introduced at position 5 of the thiazole ring, as there is an appropriate cleft in the protein binding site able to accommodate such a substituent. In addition, our analysis predicts that smaller functional groups can be attached at the meta and para positions of the phenyl ring, whereas only a small substituent can fit into the area at the ortho position. The FRET and ELISA data strongly support this binding model. In general, ortho substitutions were more active for both electron-donating and -withdrawing groups. At the ortho and meta positions, electron-withdrawing groups generally resulted in increased efficacy relative to electron-donating groups. The SAR analysis presented below is based on the FRET data, but a very similar trend is observed for the ELISA results.

The largest improvements in IC$_{50}$ were observed for ligands bearing small substituents at the ortho position of the phenyl ring. The incorporation of the chloro (**14**) and methyl (**13**) groups, which are similar in radius, at this position increases the ligand affinity about three orders of magnitude (IC$_{50}$ = 1.1 μM and 5 μM, respectively) compared to the original compounds **1–4** (IC$_{50}$ > 1 mM). Based on the calculated binding mode, substituents introduced at the ortho position approach residues 96–98 from β4
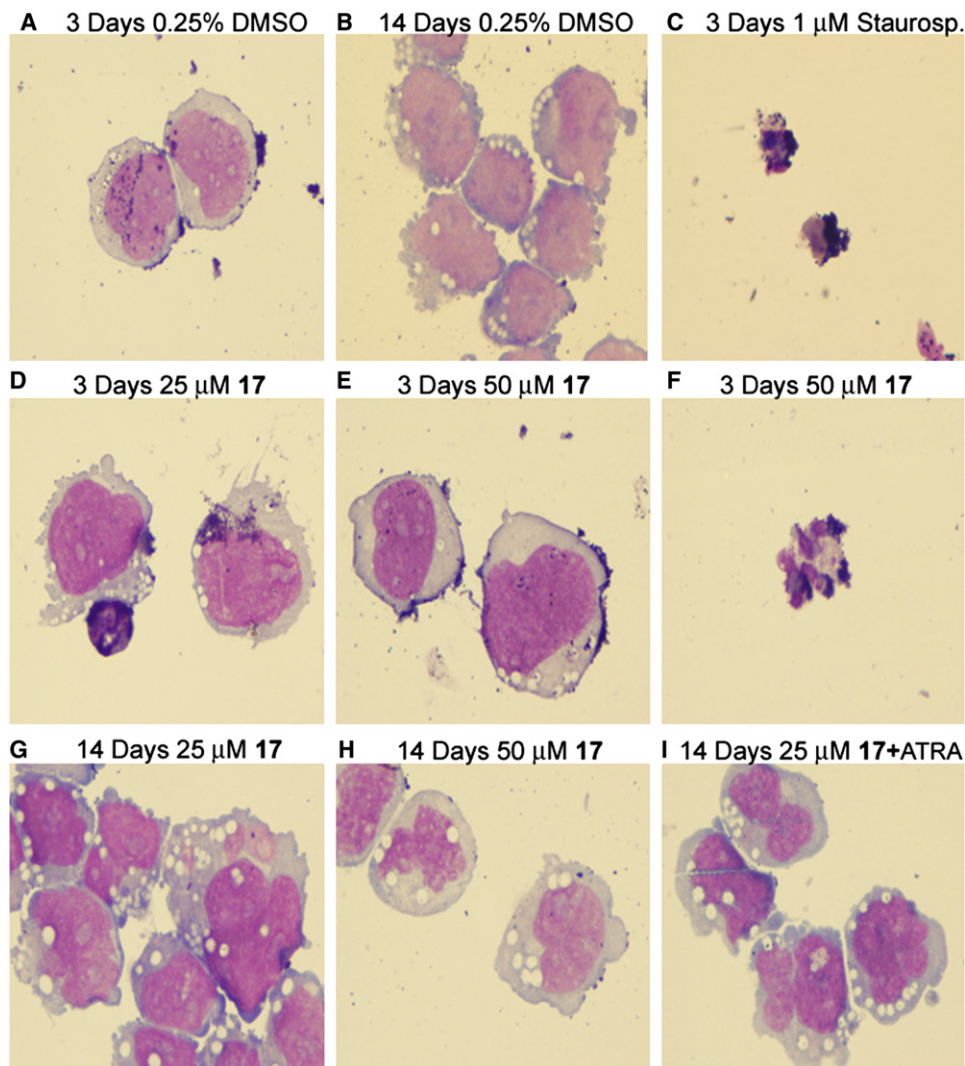
Figure 6. Morphology Changes of ME-1 Cells upon Treatment with 17

All cells were stained with Wright-Giemsa stain.

(A and B) Blast-like morphology of the ME-1 cell line seen after 3 and 14 days of treatment with the 0.25% DMSO control. Cells are uniformly large, oval, have high nuclear-cytoplasmic ratios, and a fine chromatin pattern.

(C) Apoptotic cells observed after a 3 day treatment with the protein kinase C inhibitor staurosporine.

(D–F) Similar blast-like morphology and increased apoptosis seen after 3 days of treatment with **17** at 25 μM (D) and 50 μM (E and F).

(G–I) Effects of a 14 day treatment with **17** in inducing morphologic changes of differentiation to more mature forms with variation in cell size and shape, lower nuclear-to-cytoplasmic ratio, folding and lobation of nuclei, and more clumped chromatin at 25 μM (G), 50 μM (H), and 25 μM in combination with 1 μM all-*trans*-retinoic acid (ATRA) (I).

and 111–112 from β5 (Figures 4A and 4B). The low IC_{50} values observed for these compounds can be explained by means of favorable hydrophobic interactions with the side chains of K111 and K98. A methoxy substituent at the ortho position (**15**) almost abolishes inhibition, as a result of the size and electrostatic repulsion between the oxygen atom of the methoxy group and the carbonyl oxygen of L97 (distance ~3 Å). Substituents at the meta position of the phenyl ring are directed toward residues in β4 (compounds **9**, **10**; Figure 4). Larger substituents (**11**, **12**) are directed at residues in β4 as well as the loop preceding β4 (residues 84–87). The chloro group has proven best at

this position, resulting in an IC_{50} value of 12 μM for **9**. Replacement of chloro with methyl (**10**) or methoxy (**11**) increases the IC_{50} by 9-fold and 5-fold (interactions of **10** with CBFβ are described in detail above).

No activity was observed for the compounds with larger substituents at the meta position (e.g., ethyl, dimethyl-amine group), as they cannot be accommodated in this area of the binding site. The incorporation of the trifluoro-methyl (**5**) and methoxy (**6**) groups at the para position of the phenyl ring increases the ligand affinity significantly (IC_{50} = 9 μM and 18.5 μM, respectively) compared to the parent compounds **1** and **2**. The para substituents

approach the loop connecting β3 with β4 where a small cavity is formed by E84, Y85, V86, and D87. A chloro substituent at the para position resulted in an inactive compound (data not shown), consistent with the reduced activity of **16** versus **14**. Larger substituents (e.g., ethoxy) cannot be accommodated in this area of the binding site (data not shown). Simultaneous substitution at para and meta positions by methoxy groups (**7**) reduces inhibition by 2-fold compared to single methoxy substitutions (compounds **6** and **11**), indicating that at least a part of the binding site is shared between the two groups so they cannot be well accommodated simultaneously. This is consistent with the improved activity of **8** versus **7**. Compound **8** contains a benzo[*d*] [1, 3]dioxole ring system at the corresponding positions, which makes it smaller, more rigid, and more appropriate to fit and interact with this region of the binding site.

We have also substituted at the 5 position of the thiazole ring. Incorporation of an ethyl group at this position proved to be the most effective, with an up to two orders of magnitude decrease in the IC_{50} value (compare **20** with **15**). The same substitution resulted in a 6-fold increase in potency for **17,** yielding a low micromolar ligand (IC_{50} = 3.2 μM), and a 2-fold enhancement of the binding affinity for **19** compared to the parent compounds lacking the ethyl group at the thiazole ring (**6** and **10,** respectively). A propyl group proved to be a less effective substituent at this position (**18**, IC_{50} = 23.5 μM), with no improvement in the binding affinity versus parent compound **6**. The orientation of the ligand thiazole ring in the CBFβ binding site causes the substituent at the 5 position of the thiazole ring to be positioned parallel to the backbone of the residues in β5, with G112 in closest proximity. The ethyl and propyl groups are inserted between the side chains of K111 and Y96, with both engaged in hydrophobic contacts with these substituents. The propyl group is partially solvent exposed, which may make it less effective than an ethyl at this position.

Structural Basis for Inhibition

According to the ^{15}N-^{1}H HSQC spectra of CBFβ, these compounds bind to an allosteric site displaced from the heterodimerization interface. However, for many of the compounds, we also observed perturbations of the chemical shifts for at least one of the CBFβ residues localized at the heterodimerization interface or in the vicinity thereof (Figures 4C and 4D). These residues can be categorized into two groups: amino acids located in β3 (N63, L64, Q67) and residues belonging to a loop connecting β4 with β5 (L103, N104, G105). All of these residues at the heterodimerization interface are located 10 Å or more from the ligand in our docked model, and thus it is not possible that ring current effects from the ligand could be causing these changes. Rather, the changes observed for these residues must arise indirectly from alteration of the conformation or dynamics of these residues as a result of ligand binding.

The backbone of Q67 is 4.5 Å away from the backbone of β4 residues A99 and K98, both of which are in direct contact with the allosteric ligands (Figure 4A). The proximity of Q67 to β4 likely results in an altered conformation for this residue upon ligand binding, consistent with the observed chemical shift perturbations seen with ligand binding. Structures of Runt domain-CBFβ complexes show that the side chain of Q67 is directly involved in interactions with Runt domain residues P157, N155, and F153 (Figure 4D). The energetic importance of these interactions has been demonstrated with a Q67A mutation decreasing Runt domain binding to CBFβ ~10-fold [23]. Therefore, conformational changes of Q67 induced by ligand binding may contribute to inhibition. Chemical shift changes were also observed for L64, located in the middle of β3 at the heterodimerization interface (Figure 4C). L64 is involved in intramolecular hydrophobic interactions with the side chains of W110 and L125, both of which are adjacent to the ligand binding site. The side chain of W110 is positioned close (4–5 Å) to the backbone of β5 (G112 and K113) and β6 residues (G123 and C124), which are also perturbed upon ligand binding. Conformational changes of the W110 and L125 side chains may be induced by ligand binding and propagated to L64 and L103 (the latter is involved in the same hydrophobic core; see Figure 4C). The side chain of L64 is involved in a hydrophobic interaction with Runx1 residues V159 and T149 in the complex and an L64A mutation also affects heterodimerization [23]. Again here, induced conformational changes of L64 could affect these interactions, resulting in inhibition of CBFβ heterodimerization.

Two of the perturbed residues located in the loop connecting β4 with β5, L103 and N104, have been identified as energetic "hot spots" on CBFβ binding to Runx1 [23]. These residues are in proximity to β4 residues 96–99, which are in direct contact with our allosteric ligands. In addition, L103 is part of the hydrophobic core involving W110, L125, and L64, which is affected by ligand binding (see above). Therefore, the binding of ligands to the allosteric site could easily alter the conformation and/or dynamics of this critical part of the protein (β4-β5 loop), thereby inhibiting binding of the Runx1 Runt domain to CBFβ. L103 forms hydrophobic interactions with the Runt domain residues V159 and T161 (Figure 4D) in the complex, and an L103A substitution decreases binding 5-fold [23]. N104 is involved in a hydrogen-bond network with the backbone and side chain of T161 and the backbone of V159 in the Runt domain. The importance of N104 for binding to Runx1 (an N104A substitution decreases binding ~50-fold [23]) strongly suggests that alteration of the conformation of this residue contributes to inhibition.

Our results are consistent with a model where the compounds induce changes in local conformation and/or dynamics which are transmitted through the protein to residues at the CBFβ-Runt domain interface, resulting in an altered interface which can no longer bind as effectively. This is similar to observations in other allosterically regulated proteins, where binding to allosteric sites causes conformational and/or dynamic changes at a separate functional site on the protein, resulting in altered affinity [45, 46].

Mechanism of Inhibition of ME-1 Cell Proliferation

We have shown by analysis of changes in morphology that our CBFβ inhibitors can induce increased differentiation in ME-1 cells as well as an increase in apoptosis, explaining the decrease in proliferation observed. Multiple mechanisms for these effects are possible, including release of Runx from a nonproductive Runx/CBFβ-SMMHC complex, decreased Runx binding to DNA as a result of reduced CBFβ binding (see Figure 5C), or alteration of the components present in the multiprotein Runx-DNA complex as a result of reduced CBFβ and/or CBFβ-SMMHC binding. Because the level of functional Runx present in cells has been shown to be critical for cell-cycle progression [47], any or all of these could have a substantial impact on proliferation.

SIGNIFICANCE

Numerous inhibitors of enzymatic activity have been developed; however, the development of inhibitors of protein-protein interactions has only recently come to the forefront as a viable approach. Allosteric inhibition of such protein-protein interactions presents a number of advantages, including not having to compete for binding with the partner protein, however to date there are very few examples of such inhibitors. We have developed allosteric small-molecule inhibitors of the binding of Runx1 to CBFβ. To our knowledge, these compounds represent the first small-molecule inhibitors of the protein-protein interaction between Runx1 and CBFβ. These compounds inhibit the proliferation of the human leukemia cell line ME-1, making them excellent candidates for further development. Our results clearly provide validation for development of allosteric inhibitors of protein-protein interactions as a powerful approach for achieving inhibition of these interactions.

EXPERIMENTAL PROCEDURES

Chemical Synthesis

Descriptions of the chemical syntheses are provided in the Supplemental Data.

NMR Spectroscopy

A description of the NMR spectroscopy is provided in the Supplemental Data.

FRET Assays

The His$_6$ tag and Cerulean were inserted into the pET22b vector (Novagen, Madison, WI, USA) between the NdeI and BamHI restriction sites, and the Runx1 Runt domain (Runx1 41–190) was inserted between the BamHI and XhoI sites to create the Cerulean-Runt domain fusion protein. A two amino acid linker (Gly-Ser) was included between Cerulean and Runx1. The His$_6$ tag and Venus were inserted into the pET22b vector (Novagen) between the NdeI and BamHI restriction sites, followed by CBFβ (1–141) inserted between the BamHI and XhoI sites to create the Venus-CBFβ fusion protein. A Gly-Ser linker was also included between Venus and CBFβ. The fusion proteins were purified by standard Ni-affinity chromatography. For the FRET measurements, the Cerulean-Runt and Venus-CBFβ fusion proteins were dialyzed into FRET assay buffer (25 mM Tris-HCl [pH 7.5], 150

mM KCl, 2 mM MgCl$_2$). Protein concentrations were determined by UV absorption at 433 nm for Cerulean-Runt and 513 nm for Venus-CBFβ ($\varepsilon = 34{,}000$ M^{-1}cm^{-1} and 92,200 M^{-1}cm^{-1}, respectively). Equal molar concentrations of the two proteins were mixed together, diluted to 150 nM with FRET assay buffer containing 0.1% BSA, and incubated for 1 hr. A 190 μl aliquot of the protein mixture and 10 μl of a DMSO solution of the compounds were mixed on 96-well black COSTAR (Corning Life Sciences, Lowell, MA, USA) plates and incubated at room temperature for 1 hr. A PHERAstar microplate reader (BMG Labtech, Durham, NC, USA) was used to measure fluorescence (excitation at 433 nm and emission measured at 474 and 525 nm). For IC$_{50}$ determinations, the ratios of the fluorescence intensities at 525 nm and 474 nm were plotted versus the log of compound concentration, and the resulting curve was fit to a sigmoidal curve using Origin 7.0 (MicroCal, Northampton, MA, USA). Mean values of IC$_{50}$ originating from two independent measurements performed in duplicate together with the standard deviations are reported.

ELISA Assay

A description of the ELISA for the Runt domain-CBFβ interaction is provided in the Supplemental Data.

NMR-Based Docking

A description of the NMR-based docking is provided in the Supplemental Data.

Analysis of Compound Inhibition in HEK293 Cells by FACS/FRET

A description of the FACS/FRET protocol is provided in the Supplemental Data including Figure S3.

MTT Assay of Compound Effects on Proliferation of ME-1 Cells

ME-1 cells were kindly provided by Dr. Paul Liu (NIH, Bethesda, MD, USA). ME-1 cells were grown in RPMI 1640 with Glutamax, 20% heat-inactivated fetal bovine serum, and 1% penicillin/streptomycin (Invitrogen, Carlsbad, CA, USA). The cells were plated in 90 μl in 96-well flat bottom microtiter plates (Fisher Scientific, Newark, DE, USA) at a concentration of 4×10^5/ml and treated with 0.25% sterile DMSO (Sigma, St. Louis, MO, USA), 1 μM staurosporine (Sigma), or serial dilutions of compounds from 40 mM stock solutions in DMSO. Cells were incubated in a 5% CO$_2$ incubator at 37° for 72 hr. A Vybrant MTT cell proliferation assay kit (Molecular Probes, Eugene, OR, USA) was used with addition of 10 μl of 12 mM MTT solution to each well followed by incubation at 37°C for an additional 4 hr. One hundred microliters of sodium dodecyl sulfate in 0.01 M HCl was added to each well and incubated at 37°C overnight. Plates were read for absorbance at 570 nm using a PHERAstar BMG microplate reader. Mean values and standard deviations were determined from two independent experiments, each performed in quadruplicate, for each condition.

Runx1 ELISA for DNA Binding

An ELISA was run using an AML-1/Runx1 transcription factor assay kit purchased from Active Motif (Carlsbad, CA, USA) using the manufacturer's protocol in order to determine DNA binding by measurement of UV absorbance at 450 nm. Five micrograms of HL60 nuclear extract from Active Motif was added to each with the exception of the negative control, which contained only nuclear extract and binding buffers. One hundred percent DMSO and 40 mM **17** in DMSO were diluted in nuclear extract buffer and added to attain final concentrations of 0.25% DMSO and 100 μM **17** in 0.25% DMSO. The mixtures were incubated for 1 hr at room temperature. Each condition was repeated five times.

Supplemental Data

Supplemental Data include four figures, one table, and Supplemental Experimental Procedures and can be found with this article online at http://www.chembiol.com/cgi/content/full/14/10/1186/DC1/. Table S1 and Figures S1 and S2 show results of NMR CSP-based docking

for compound **10**. A description of the procedure employed for FACS/FRET in HEK293 cells is provided in Figure S3. Descriptions of the ELISA assay and the testing of **17** against the Hep-G2, HK-2, K562, HL60, and U937 cell lines (Figure S4) are provided. Descriptions of the synthesis and characterization for all compounds are provided. The Protein Data Bank format coordinates for **10** docked to CBFβ are also provided.

REFERENCES

1. Speck, N.A., Stacy, T., Wang, Q., North, T., Gu, T.L., Miller, J., Binder, M., and Marin-Padilla, M. (1999). Core-binding factor: a central player in hematopoiesis and leukemia. Cancer Res. *59*, 1789s–1793s.

2. Gu, T.L., Goetz, T.L., Graves, B.J., and Speck, N.A. (2000). Auto-inhibition and partner proteins, core-binding factor β (CBFβ) and Ets-1, modulate DNA binding by CBFα2 (AML1). Mol. Cell. Biol. *20*, 91–103.

3. Huang, G., Shigesada, K., Ito, K., Wee, H.J., Yokomizo, T., and Ito, Y. (2001). Dimerization with PEBP2β protects RUNX1/AML1 from ubiquitin-proteasome-mediated degradation. EMBO J. *20*, 723–733.

4. Liu, P., Tarle, S.A., Hajra, A., Claxton, D.F., Marlton, P., Freedman, M., Siciliano, M.J., and Collins, F.S. (1993). Fusion between transcription factor CBF β/PEBP2 β and a myosin heavy chain in acute myeloid leukemia. Science *261*, 1041–1044.

5. Castilla, L.H., Wijmenga, C., Wang, Q., Stacy, T., Speck, N.A., Eckhaus, M., Marin-Padilla, M., Collins, F.S., Wynshaw-Boris, A., and Liu, P.P. (1996). Failure of embryonic hematopoiesis and lethal hemorrhages in mouse embryos heterozygous for a knocked-in leukemia gene CBFB-MYH11. Cell *87*, 687–696.

6. Lukasik, S.M., Zhang, L., Corpora, T., Tomanicek, S., Li, Y., Kundu, M., Hartman, K., Liu, P.P., Laue, T.M., Biltonen, R.L., et al. (2002). Altered affinity of CBFβ-SMMHC for Runx1 explains its role in leukemogenesis. Nat. Struct. Biol. *9*, 674–679.

7. Toogood, P.L. (2002). Inhibition of protein-protein association by small molecules: approaches and progress. J. Med. Chem. *45*, 1543–1558.

8. Gadek, T.R., and Nicholas, J.B. (2003). Small molecule antagonists of proteins. Biochem. Pharmacol. *65*, 1–8.

9. Cochran, A.G. (2000). Antagonists of protein-protein interactions. Chem. Biol. *7*, R85–R94.

10. Cochran, A.G. (2001). Protein-protein interfaces: mimics and inhibitors. Curr. Opin. Chem. Biol. *5*, 654–659.

11. Teague, S.J. (2003). Implications of protein flexibility for drug discovery. Nat. Rev. Drug Discov. *2*, 527–541.

12. Meagher, K.L., and Carlson, H.A. (2004). Incorporating protein flexibility in structure-based drug discovery: using HIV-1 protease as a test case. J. Am. Chem. Soc. *126*, 13276–13281.

13. Gao, Y., Dickerson, J.B., Guo, F., Zheng, J., and Zheng, Y. (2004). Rational design and characterization of a Rac GTPase-specific small molecule inhibitor. Proc. Natl. Acad. Sci. USA *101*, 7618–7623.

14. Wang, J.L., Liu, D., Zhang, Z.J., Shan, S., Han, X., Srinivasula, S.M., Croce, C.M., Alnemri, E.S., and Huang, Z. (2000). Structure-based discovery of an organic compound that binds Bcl-2 protein and induces apoptosis of tumor cells. Proc. Natl. Acad. Sci. USA *97*, 7124–7129.

15. Degterev, A., Lugovskoy, A., Cardone, M., Mulley, B., Wagner, G., Mitchison, T., and Yuan, J. (2001). Identification of small-molecule inhibitors of interaction between the BH3 domain and Bcl-xL. Nat. Cell Biol. *3*, 173–182.

16. Berg, T., Cohen, S.B., Desharnais, J., Sonderegger, C., Maslyar, D.J., Goldberg, J., Boger, D.L., and Vogt, P.K. (2002). Small-molecule antagonists of Myc/Max dimerization inhibit Myc-induced transformation of chicken embryo fibroblasts. Proc. Natl. Acad. Sci. USA *99*, 3830–3835.

17. Poy, F., Lepourcelet, M., Shivdasani, R.A., and Eck, M.J. (2001). Structure of a human Tcf4-β-catenin complex. Nat. Struct. Biol. *8*, 1053–1057.

18. DeDecker, B.S. (2000). Allosteric drugs: thinking outside the active-site box. Chem. Biol. *7*, R103–R107.

19. Horn, J.R., and Shoichet, B.K. (2004). Allosteric inhibition through core disruption. J. Mol. Biol. *336*, 1283–1291.

20. Last-Barney, K., Davidson, W., Cardozo, M., Frye, L.L., Grygon, C.A., Hopkins, J.L., Jeanfavre, D.D., Pav, S., Qian, C., Stevenson, J.M., et al. (2001). Binding site elucidation of hydantoin-based antagonists of LFA-1 using multidisciplinary technologies: evidence for the allosteric inhibition of a protein-protein interaction. J. Am. Chem. Soc. *123*, 5643–5650.

21. McMillan, K., Adler, M., Auld, D.S., Baldwin, J.J., Blasko, E., Browne, L.J., Chelsky, D., Davey, D., Dolle, R.E., Eagen, K.A., et al. (2000). Allosteric inhibitors of inducible nitric oxide synthase dimerization discovered via combinatorial chemistry. Proc. Natl. Acad. Sci. USA *97*, 1506–1511.

22. Huang, X., Peng, J.W., Speck, N.A., and Bushweller, J.H. (1999). Solution structure of core binding factor β and map of the CBF α binding site. Nat. Struct. Biol. *6*, 624–627.

23. Tang, Y.Y., Shi, J., Zhang, L., Davis, A., Bravo, J., Warren, A.J., Speck, N.A., and Bushweller, J.H. (2000). Energetic and functional contribution of residues in the core binding factor β (CBFβ) subunit to heterodimerization with CBFα. J. Biol. Chem. *275*, 39579–39588.

24. Bohm, H.J. (1998). Prediction of binding constants of protein ligands: a fast method for the prioritization of hits obtained from de novo design or 3D database search programs. J. Comput. Aided Mol. Des. *12*, 309–323.

25. Bohm, H.J. (1992). The computer program LUDI: a new method for the de novo design of enzyme inhibitors. J. Comput. Aided Mol. Des. *6*, 61–78.

26. Hajduk, P.J., Meadows, R.P., and Fesik, S.W. (1999). NMR-based screening in drug discovery. Q. Rev. Biophys. *32*, 211–240.

27. Fejzo, J., Lepre, C., and Xie, X. (2003). Application of NMR screening in drug discovery. Curr. Top. Med. Chem. *3*, 81–97.

28. Rudisser, S., and Jahnke, W. (2002). NMR and in silico screening. Comb. Chem. High Throughput Screen. *5*, 591–603.

29. Leone, M., Crowell, K.J., Chen, J., Jung, D., Chiang, G.G., Sareth, S., Abraham, R.T., and Pellecchia, M. (2006). The FRB domain of mTOR: NMR solution structure and inhibitor design. Biochemistry *45*, 10294–10302.

30. Dodson, R.M., and King, L.C. (1945). The reaction of ketones with halogens and thiourea. J. Am. Chem. Soc. *67*, 2242–2243.

31. King, L.C., and Hlavacek, R.J. (1950). The reaction of ketones with iodine and thiourea. J. Am. Chem. Soc. *72*, 3722–3724.

32. Feng, B.Y., Shelat, A., Doman, T.N., Guy, R.K., and Shoichet, B.K. (2005). High-throughput assays for promiscuous inhibitors. Nat. Chem. Biol. *1*, 146–148.

33. Wyss, D.F., Arasappan, A., Senior, M.M., Wang, Y.S., Beyer, B.M., Njoroge, F.G., and McCoy, M.A. (2004). Non-peptidic small-molecule inhibitors of the single-chain hepatitis C virus NS3 protease/NS4A cofactor complex discovered by structure-based NMR screening. J. Med. Chem. *47*, 2486–2498.

34. McCoy, M.A., and Wyss, D.F. (2000). Alignment of weakly interacting molecules to protein surfaces using simulations of chemical shift perturbations. J. Biomol. NMR *18*, 189–198.

35. Chan, F.K., and Holmes, K.L. (2004). Flow cytometric analysis of fluorescence resonance energy transfer: a tool for high-throughput screening of molecular interactions in living cells. Methods Mol. Biol. *263*, 281–292.

36. Chan, F.K., Siegel, R.M., Zacharias, D., Swofford, R., Holmes, K.L., Tsien, R.Y., and Lenardo, M.J. (2001). Fluorescence resonance energy transfer analysis of cell surface receptor interactions and signaling using spectral variants of the green fluorescent protein. Cytometry *44*, 361–368.

37. Horvath, G., Petras, M., Szentesi, G., Fabian, A., Park, J.W., Vereb, G., and Szollosi, J. (2005). Selecting the right fluorophores and flow cytometer for fluorescence resonance energy transfer measurements. Cytometry A *65*, 148–157.

38. He, L., Grammer, A.C., Wu, X., and Lipsky, P.E. (2004). TRAF3 forms heterotrimers with TRAF2 and modulates its ability to mediate NF-κB activation. J. Biol. Chem. *279*, 55855–55865.

39. van Wageningen, S., Pennings, A.H., van der Reijden, B.A., Boezeman, J.B., de Lange, F., and Jansen, J.H. (2006). Isolation of FRET-positive cells using single 408-nm laser flow cytometry. Cytometry A *69*, 291–298.

40. Hashimoto, A., Hirose, K., and Iino, M. (2005). BAD detects coincidence of G2/M phase and growth factor deprivation to regulate apoptosis. J. Biol. Chem. *280*, 26225–26232.

41. Doucey, M.A., Goffin, L., Naeher, D., Michielin, O., Baumgartner, P., Guillaume, P., Palmer, E., and Luescher, I.F. (2003). CD3 δ establishes a functional link between the T cell receptor and CD8. J. Biol. Chem. *278*, 3257–3264.

42. Yanagisawa, K., Horiuchi, T., and Fujita, S. (1991). Establishment and characterization of a new human leukemia cell line derived from M4E0. Blood *78*, 451–457.

43. Yanagisawa, K., Sato, M., Horiuchi, T., Hasegawa, H., and Fujita, S. (1994). Difference in response to colony-stimulating factors and involvement of protein kinase C signal transduction system in three subclones from the ME-1 cell line and two sublines. Blood *84*, 84–93.

44. Yanagisawa, K., Watanabe, I., Inoue, Y., Horiuchi, T., Hasegawa, H., Yasukawa, M., and Fujita, S. (1996). Diverse effects of tumor necrosis factor-α on three subclones from human myelomonocytic leukemia cell line ME-1 exhibiting different differentiation stages. J. Interferon Cytokine Res. *16*, 685–693.

45. Yan, J., Liu, Y., Lukasik, S.M., Speck, N.A., and Bushweller, J.H. (2004). CBFβ allosterically regulates the Runx1 Runt domain via a dynamic conformational equilibrium. Nat. Struct. Mol. Biol. *11*, 901–906.

46. Hardy, J.A., and Wells, J.A. (2004). Searching for new allosteric sites in enzymes. Curr. Opin. Struct. Biol. *14*, 706–715.

47. Bernardin-Fried, F., Kummalue, T., Leijen, S., Collector, M.I., Ravid, K., and Friedman, A.D. (2004). AML1/RUNX1 increases during G1 to S cell cycle progression independent of cytokine-dependent phosphorylation and induces cyclin D3 gene expression. J. Biol. Chem. *279*, 15678–15687.